Biosensors and Bioelectronics 46 (2013) 1–7

Contents lists available at SciVerse ScienceDirect

Biosensors and Bioelectronics

journal homepage: www.elsevier.com/locate/bios

Fabrication of an ultrasensitive electrochemical immunosensor for CEA based on conducting long-chain polythiols

Zhimin Liu, Zhanfang Ma *

Department of Chemistry, Capital Normal University, Beijing 100048, China

ARTICLE INFO

Article history:
Received 16 January 2013
Accepted 13 February 2013
Available online 21 February 2013

Keywords:
Poly (2-aminothiophenol)
Long-chain polythiols
Gold nanoparticles
Amperometric immunosensor
Carcinoembryonic antigen

ABSTRACT

A conducting long-chain polythiols (poly (2-aminothiophenol), PATP) was synthesized by a chemical polymerization process and combined with Au nanoparticles (AuNPs) to prepare a novel, sensitive and label-free electrochemical biosensor by adsorption of carcinoembryonic antibody (anti-CEA) on the PATP–AuNPs modified gold electrode. Differential pulse voltammetry (DPV) was used to characterize the recognition of carcinoembryonic antigen (CEA). Under the optimized conditions, the proposed immunosensor displayed a good amperometric response to CEA with linear range from 1 fg mL^{-1} to 10 ng mL^{-1} and a detection limit of 0.015 fg mL^{-1} (signal/noise = 3). The results demonstrated that the immunosensor has advantages of high sensitivity, wide linear range, good repeatability, and good selectivity. Importantly, the results of the detection of clinical serum specimens with the proposed sensor were well consistent with the data determined by micropartical enzyme immunoassay (MPEI), showing that the present work provides a promising ultrasensitive immunoassay strategy for clinical applications.

1. Introduction

Electrochemical biosensors have shown potential for fast, accurate and sensitive health care monitoring at a patient's bedside (Wang, 2006; Wang et al., 2012; Shi and Ma, 2010; Wang et al., 2013). In general, an electrochemical biosensor consists of a biological layer which is connected to a transducer system by a chemical interface layer. Since this chemical layer constitutes the interface with the sample, which strongly determines the stability, specificity, sensitivity, and repeatability of the sensor as a whole. Many efforts have been made toward the exploration of novel matrices for the fabrication of electrochemical biosensor. Successful strategies include the employment of polyethylene glycol and its derivatives (Masson et al., 2005), chitosan (Wu et al., 2006), poly (ethyleneimine) (Pchelintsev et al., 2009), nafion (Tsai et al., 2005), poly (allylamine hydrochloride) (Noguchi and Anzai, 2006), organic thiols (Thipmanee et al., 2012), etc.

Among these substrate materials, organic thiols have attracted much interest as suitable matrices in the electronic, optical, and microgravimetric transduction of different biomolecular recognition events (Nuzzo et al., 1987; Xiao and Yu, 2010; de Boer et al., 2003; Mustafa et al., 2012). Because they exhibit excellent properties for this particular purpose, including easy preparation, formation of strong specific interaction with Au nanoparticles (AuNPs), easy deposition on the electrode to form monolayers, desirable biocompatibility, and easy modification by other functional groups (Larson-Smith and Pozzo, 2012; Bain et al., 1989; Vercelli et al., 2007; Kyprianou et al., 2010). In particular, the chain length of organic thiols impacts the performance such as the stability and sensitivity of the immunosensors due to the long-chain thiols (with 10 or more carbon atoms per alkyl chain) were prefer to adopt the standing up configuration which can provide a larger number of receptors, while the short-chain thiols dominate a lying down surface structure (Crooks and Ricco, 1998; Porter et al., 1987; Addato et al., 2011; Rouhana et al., 2011; Vitaliano et al., 2009). Riepl et al. (1999) fabricated a sensor based on gold–alkanethiol system with different thiols and demonstrated that the use of longer-chain thiols enhanced the sensitivity for detection of mouse IgG. Significantly, organic thiols have been widely used as matrices for analytical signal amplification (Porter et al., 1987; Yang et al., 2005; Lawson and Huser, 2012). However, some disadvantages of long-chain thiols still obstruct the widely applications in the biosensors. Although the long-chain thiols are more stable than the short-chain ones, the dissociation of the gold–sulfur binding is also a critical issue leading to operative errors of sensors (Cai and Baldelli, 2011). In addition, it was found that the electron transfer rate of redox molecules was decreased exponentially with the increase of the alkyl chain length of the monolayer for both inner and outer sphere reactions (Xiao et al., 2009).

In order to improve the stability and conductivity of the long-chain thiols, we synthesized a novel polymer, poly (2-aminothiophenol) (PATP), which is a derivative of polyaniline contained 25

* Corresponding author. Tel.: +86 10 68902491.
E-mail address: mazhanfang@yahoo.com (Z. Ma).

0956-5663/$ - see front matter © 2013 Elsevier B.V. All rights reserved.
http://dx.doi.org/10.1016/j.bios.2013.02.016

repeated units and multiple thiol groups. The obtained PATP can easily to form a stable thin film and provide tenacious attachment to AuNPs or GE surfaces due to the cooperative binding through multiple thiols bonds (Johnson and Levicky, 2003; Sun et al., 1994). Significantly, the remnant (unbound) thiols moieties of PATP can provide reactive sites for modification with AuNPs to fix more antibodies which can enhance the sensitivity of immunosensors. Moreover, the good conductivity can further enhance the sensitivity of immunosensors since the PATP acts as an effective mediator for electron transfer in redox (Luo and Do, 2004). Owing to these advantages, the PATP is successfully used to fabricate a simple, label-free, and ultrasensitive electrochemical immunosensor for carcinoembryonic antigen (CEA) detection. The immunosensor exhibited high sensitivity, wide linear range (1 fg mL^{-1}–10 ng mL^{-1}), low detection limit (0.015 fg mL^{-1}). In addition, the results of clinical serum specimens determined by this immunosensor received a good agreement with the reference values.

2. Experimental section

2.1. Reagents and chemicals

CEA and anti-CEA were purchased from Beijing Biosynthesis Biotechnology Co. Ltd. (Beijing, China). Hydrogen tetrachloroaurate (III) hydrate ($HAuCl_4 \cdot XH_2O$), D-(+)-glucose, ascorbic acid (AA), uric acid (UA), α-1-fetoprotein (AFP), ammonium peroxidisulfate (APS) and 2-aminothiophenol (ATP) were achieved from Alfa Aesar (Tianjin, China). 2-methylaziridine (MA), Human immunoglobulin G (IgG), and albumin from bovine serum (BSA) were purchased from Chengwen Biological Company (Beijing, China). Sodium citrate (99%), KH_2PO_4 (99%), HCl, Na_2HPO_4 (99%), N,N-dimethyl formamide (DMF), N-Methyl-2-pyrrolidinone (NMP) and KCl (99.5%) were obtained from Beijing Chemical Reagents Company (Beijing, China). $K_4Fe(CN)_6$ (99%) and $K_3Fe(CN)_6$ (99%) were obtained from Sinopharm Chemical Reagent Co. Ltd. (Shanghai, China). Sodium borohydride ($NaBH_4$, 98%) was purchased from Sigma (USA). Clinical serum samples were provided by the hospital of our university. All chemicals were of analytical grade and used without further purification, and distilled water was used throughout.

2.2. Apparatus

All electrochemical measurements were performed with a CHI-832 electrochemical analyzer (Chenhua, Shanghai, China). A three-electrode electrochemical cell was composed of a modified gold electrode (GE, $\Phi=2$ mm) as the working electrode, a platinum wire as the auxiliary electrode, and an Ag/AgCl electrode (saturation of KCl) as the reference electrode. Electrochemical impedance spectroscopy (EIS) was measured from 200 kHz to 0.01 Hz by Advanced Electrochemical System of PARSTAT 2273 (Princeton Co., USA). The size of gold nanoparticles was estimated from transmission electron microscopy (TEM) (H600, Hitachi Instrument, Japan). The number density of 5 nm AuNPs was 5.47×10^{13} mL^{-1} (the calculating method was indicated in Supplementary information). The $K_4[Fe(CN)]_6/K_3[Fe(CN)]_6$ mixture solution (1:1, 5 mM) used in differential pulse voltammetry (DPV) measurements was prepared by 0.1 M phosphate buffer solution (PBS) of pH 5.29. The clinical serum specimens were assayed using the commercial micropartical enzyme immunoassay (MPEI). The structure and conductivity of PATP was studied by Fourier transform infrared spectroscopy (FTIR) and four-probe method (keithley 6221/2182A, USA), respectively.

GEs were immersed in piranha solution (3/1, V/V, concentrated H_2SO_4/30% H_2O_2) for 2 h, and then polished successively in 1.0, 0.3, and 0.05 μm alumina slurries. The electrodes were thoroughly rinsed with pure water and sonicated in pure water for 5 min between polishing steps. Before modification, the electrodes were dried with nitrogen gas.

The viscosity of the conducting polymer in the linear viscoelastic regime was carried with a stress-controlled rheometer of TA Instruments (AR-2000ex, TA, USA). The lower fixture incorporated a concentric cylinder, providing temperature control, while the upper fixture was equipped with a parallel cylinder of a diameter of 40 mm. For all cases, the linear response was fixed at 10% of strain amplitude. In addition, the dynamic frequency-sweep measurements at $\omega=0.4642-21.54$ rad/s were also made repeatedly (from high ω to low ω) at 25 °C.

2.3. Preparation of AuNPs

The AuNPs with the sizes of 5, 10, 15, and 25 nm used in this work were prepared according to a literature (Frens, 1973) with slight modifications. 5 nm AuNPs were prepared at room temperature by adding 1 mL 1% sodium citrate solution to the 100 mL 0.01% $HAuCl_4$ aqueous solution with stirring. After 1 min, 1.6 mL 0.075% $NaBH_4$ (dissolved in 1% sodium citrate solution) was added. The mixture was kept stirring until its color turned to red. For 10 nm AuNPs, the preparing procedures were the same as that of 5 nm except the addition of 1 mL $NaBH_4$ solution. For 15, 25, and 40 nm AuNPs, they were obtained by adding 5, 3.2, and 2 mL 1% sodium citrate solution, respectively, to 100 mL 0.01% boiling aqueous $HAuCl_4$ solution with vigorous stirring. The color changed from pale to blue, then to burgundy. Boiling was continued for 15 min and kept stirring until the sample had cooled to room temperature. All the AuNPs were stored at 4 °C for use.

2.4. Preparation of the PATP

The functional polyaniline was synthesized according to the reported method with some modifications by using ammonium peroxidisulfate as oxidant in the presence of HCl (Sergeyeva et al., 1996). In general, 1.1141 g APS was added into the 2-aminothiophenol solutions in 1 M HCl with stirring at room temperature. After the polymerization for 24 h, the PATP was obtained (Fig. S1 in supplementary information). The product was separated by filtration and purified by repeated washing with water and acetone to remove the residual oxidant and oligomers. Then the precipitate was dried in vacuum at 60 °C for 12 h. After the solvent had been evaporated, the powder was stored at 4 °C for use.

Some of the polymer powder was dissolved in DMF so that the PATP solution can be used to modify the gold electrode.

2.5. Preparation of modified electrode

The pretreated gold electrode was cast with 1.2 μL brown solution of PATP at room temperature for 8 h to adsorb the conducting long-chain polythiols. After that, the electrode thoroughly rinsed with deionized water and dried under a stream of nitrogen gas. Subsequently, it was immersed in AuNPs solution for 8 h. Then the GE-PATP-AuNPs was dipped into a solution of anti-CEA (200 μg mL^{-1} in 0.1 M phosphate buffer (PB), pH 7.3) for 6 h at 4 °C to absorb the antibodies (GE–PATP–AuNPs–anti-CEA). Finally, the modified immunosensor was incubated in a solution of BSA (1%, w/w) for about 1 h at 37 °C. The immunosensor was stored at 4 °C for use.

3. Results and discussion

3.1. Characterization of PATP

FTIR was used to characterize the structure of PATP (Fig. S2 in supplementary information). The characteristic peaks at 1473 and 1529 cm^{-1} are assigned to the C=C stretching modes of benzenoid and quinonoid rings, respectively (Zengin et al., 2002). The band corresponding to C–S stretching vibration is observed at 761 cm^{-1}. Additionally, the peak at 2576 cm^{-1} comes from S–H stretching vibrations, revealing that the hydrosulphonyl had not been oxidized (Han et al., 2011). The results confirm the formation of conducting polymer PATP.

The weight average molecular weight of PATP was calculated as 3130 g mol^{-1} based on the value of intrinsic viscosity (0.059 dL g^{-1}, Fig. S3 in supplementary information), which means the polymeric chain was made up of 25 repeated units. Moreover, the conductivity of PATP has been measured by four-probe method, which was 2.2×10^{-5} S cm^{-1}.

3.2. Principles of the immunosensor

The membrane of PATP was firstly attached to the surface of the GE and then adsorbed AuNPs. The PATP contained long chain and multiple thiol groups, which can be used to improve the stability of the PATP–GE and PATP–AuNPs interfaces. The polythiols played an important role in immobilizing AuNPs so that there were more sites for the attachment of anti-CEA, which improved the sensitivity of the immunosensor. Moreover, the conductivity of the PATP and AuNPs was propitious to the electron transfer and resulted in the improvement of the sensitivity of detecting CEA. The incubation of the modified immunosensor in BSA solution at 37 °C for 1 h blocked any remaining active sites, which eliminated non-specific adsorption. The steps including electrode modification and anti-CEA attachments are shown in Scheme 1. CEA could be immobilized on GE surface modified with anti-CEA through the immunorecognition, which was expected to attenuate the electrochemical activity and decrease the current of immunosensor. DPV was used to monitor the attachment of each component. Based on this, the immunosensor can be used in quantitative detection.

3.3. DPV characterization of modified electrodes

DPV experiments of modified electrodes were performed in 5 mM $K_3[Fe(CN)_6]/K_4[Fe(CN)_6]$–PBS (pH 5.29) from 0 to 0.5 V (vs. Ag/AgCl) at a scan rate of 50 mV s^{-1} as shown in Fig. 1A. The peak current was observed at bare GE in potential range was about 60 μA (curve a). After PATP was coated on the GE surface, the current peak was considerably reduced to approximately 20 μA (curve b), which was ascribed to that the conductivity of PATP is not as good as bare GE. With the dropping of AuNPs solution the peak current increase significantly (curve c), which was higher than bare GE. That is because not only the conductivity of AuNPs is better than PATP but also the AuNPs fixed on the long-chain polythiols would increase the area of electrode. When the electrode was modified with anti-CEA, the peak current was decreased (curve d). Subsequently, the immunosensor was blocked with 1% BSA solution and then incubated in a solution containing 1 pg mL^{-1} CEA. It could be found that the peak currents of the curves (e) and (f) were decreased comparing with curve (d). The reason was that the insulating BSA and CEA protein layers on

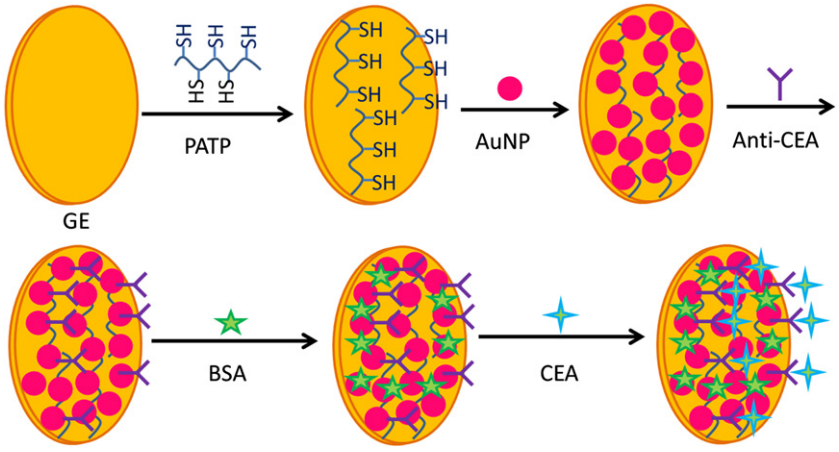

Scheme 1. Fabrication of immunosensor and immunological recognition between anti-CEA and CEA.

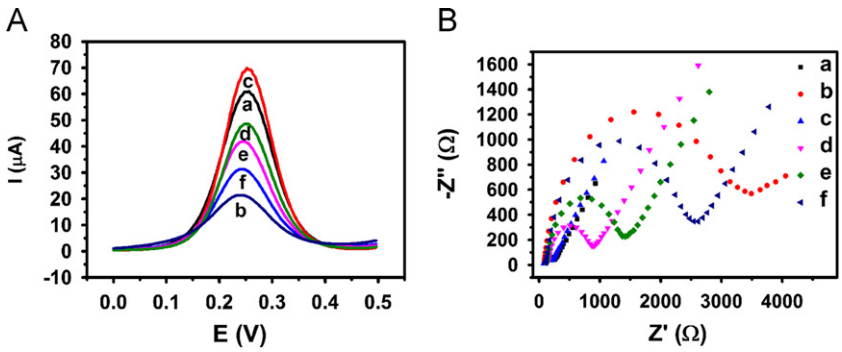

Fig. 1. DPV (A) and EIS (B) of the GEs modified with (a) bare GE, (b) PATP, (c) PATP–AuNPs, (d) PATP–AuNPs–anti-CEA, (e) PATP–AuNPs–anti-CEA blocked with 1% BSA, and (f) PATP–AuNPs–anti-CEA incubated with 1 pg mL^{-1} CEA after blocked with 1% BSA. All the experiments were performed in 5 mM $K_3[Fe(CN)_6]/K_4[Fe(CN)_6]$–PBS (pH 5.29).

the electrode retarded the electron transfer. These results showed that the anti-CEA were successfully immobilized on GE.

3.4. EIS characterization of the interfacial properties of modified electrodes

EIS was used to demonstrate the interfacial properties of physicochemical process in different modification-layers. It consists of two portions: the semicircle portion and the linear portion. The semicircle diameter at higher part represents the electron-transfer resistance (R_{et}), and the linear part at lower frequencies represents the diffusion process. Fig. 1B shows the Nyquist plots of EIS observed upon the stepwise modification processes. It was observed that the variation tendency of R_{et} of EIS plots was opposite to the peak current of DPV plots in different modification process.

The equivalent electrical circuit (Fig. S4 in supplementary information) was chosen to fit the impedance data obtained from modification process, where R_s is the solution resistance, R_{et} is the electron-transfer resistance, C_{dl} is the double layer capacitance, R_{film} and C_{film} is the resistance and capacitance of PATP film, respectively. From the data of EIS, it was determined that the PATP–AuNPs modified electrode (Fig. 1B, curve c) exhibited a smaller electron-transfer resistance than that of bare GE (curve a in Fig. 1B), which revealed the ferrocyanide was dominating converted at the AuNPs. Additionally, comparisons of EIS of GE modified with ATP and PATP were performed. It was observed that the R_{et} of PATP modified GE was much smaller than that of ATP modified electrode (Fig. S5A in supplementary information), suggesting that the conductivity of PATP was much better. It could also be found that the R_{et} of GE modified with ATP–AuNPs was larger than that of PATP–AuNPs modified GE (Fig. S5B in supplementary information), showing that the PATP adsorbed more AuNPs.

3.5. Optimization of analytical conditions

3.5.1. Influences of the pH of $K_3[Fe(CN)_6]/K_4[Fe(CN)_6]$–PBS electrolyte solution on immunosensorelectrolyte solutionelectrolyte solution

It was well known that the pH of the solution has a profound effect on the amperometric responses. In order to optimize the pH, a series of $K_3[Fe(CN)_6]/K_4[Fe(CN)_6]$–PBS solutions with the pH from 4.92 to 8.34 were prepared. The immunosensors was blocked with 1% BSA solution (Fig. 2A) and then incubated in a solution containing 1 pg mL^{-1} CEA (Fig. 2B). It was found that the amperometric responses in Fig. 2A decreased as pH increase in the range from 4.92 to 8.34. However, in Fig. 2B, the changes of oxidation peak current responses (ΔI) increased in the pH range from 4.92 to 5.29 and then decreased as pH increase. For the curve of Fig. 2A, that was because the conductivity of polyaniline and its derivatives were known to be essentially pH-dependent. But the experimental results of immunoassay indicated that there is the best sensitivity at pH 5.29. In this case, the pH of 5.29 was used in the further study.

3.5.2. Influences of concentration of the PATP solution

The effect of concentration of the PATP solution was studied. The pretreated gold electrode was cast with 1.2 μL brown solution of PATP (5, 2, 1, 0.5, 0.2, 0.1, 0.05 g L^{-1}) at room temperature for 8 h to adsorb the conducting polymer. Then the electrodes were immersed in AuNPs, anti-CEA, and 1% BSA solutions successively. The typical DPV plots were recorded in Fig. 3A. It could be observed that the amperometric responses increased in the concentration range from 0.05 to 0.5 g L^{-1} and then decreased as concentration increase further. The experimental results indicated that the maximum response occurred at 0.5 g L^{-1}.

3.5.3. Influences of the size and amount of AuNPs

As well known, nanoscaled gold particles have some important size-dependent properties due to the quantum size effect. The AuNPs with 5, 10, 15, 25, and 40 nm in diameter were used to fabricate the GE–PATP–AuNPs electrode. Fig. 3B reveals the influence of size of the immunosensors. It could be observed the response signals decreased with the increasing AuNPs size. This is because the surface of metallic nanoparticles is always electron-deficient, and the affinity to electrons would increase with the decrease of dimension (Henglein et al., 1991). As the diameter of the AuNPs reduced to 5 nm, the AuNPs could act as strong electron acceptors to adsorb electrons from $[Fe(CN)_6]^{4-}$; thus, oxidation of ferricyanide was catalyzed, leading to the increase of anodic peak current. Despite the potential advantages associated with enhanced affinity to electrons, ultrasmall AuNPs (<5 nm) have been used less frequently in biosensor fabrication than the larger ones (i.e. ≥ 5 nm in diameter) (Robinson et al., 2000; Giberson and Demaree, 1994; Yokota, 1988). A major reason for this is the fact that the ultrasmall AuNPs are difficult to prepare or tend to aggregate (Santos et al., 2005; Hartlen et al., 2012). So the size smaller than 5 nm was not studied here and 5 nm AuNPs were adopted for subsequent study.

Besides the size, the amount of AuNPs played an important role in the performance of the immunosensors. As shown in Fig. S6 (in supplementary information), the amperometric responses increased in the amount range from 1 to 3 μL at 5.47×10^{13} mL^{-1} of the number density for 5 nm AuNPs. For more than 3 μL Au NPs used, the amperometric responses reached maximum value and tended to level off, showing that most of available thiols sites were bound by AuNPs.

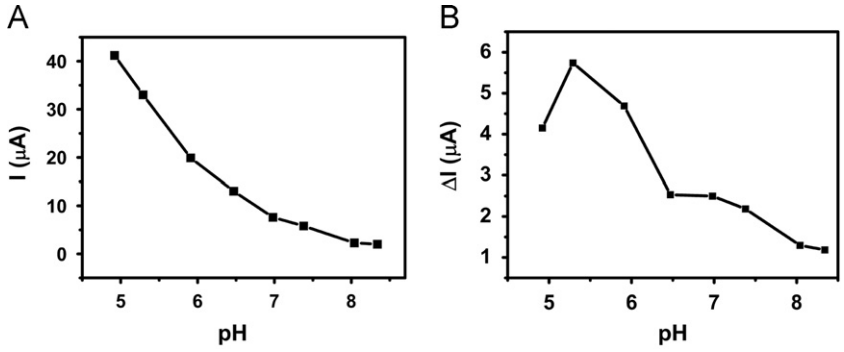

Fig. 2. pH dependency of the anodic peak currents responses for the inmunosensor in 5 mM $K_3[Fe(CN)_6]/K_4[Fe(CN)_6]$–PBS at 50 mV s^{-1} scan rate before (A) and after incubation with 1 pg mL^{-1} CEA (B).

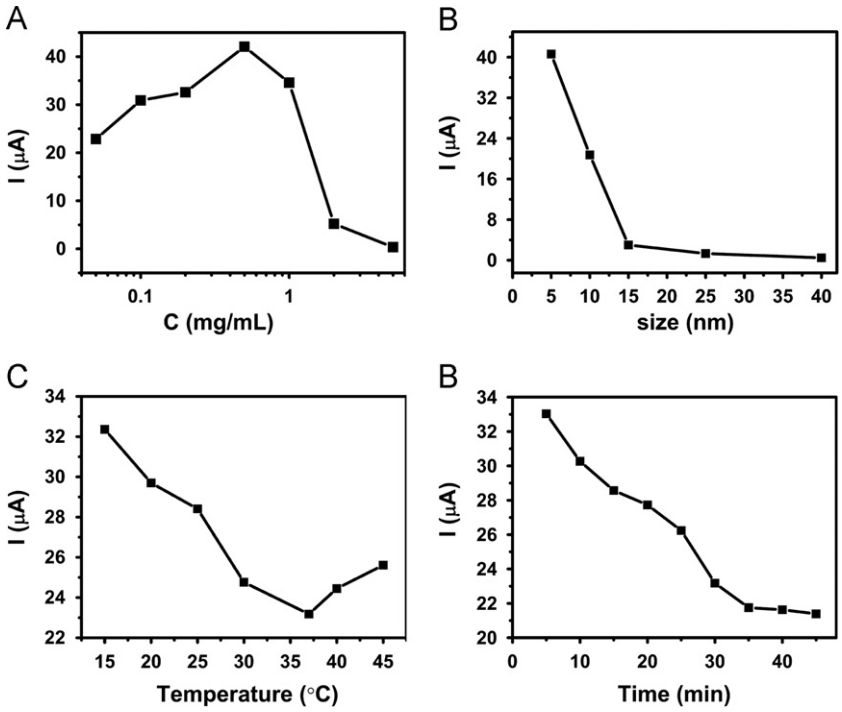

Fig. 3. The effects of different conditions on amperometric response of immunosensor: (A) PATP concentration; (B) AuNPs size; (C) incubation temperature and (D) incubation time after immunosensor incubated with 1 ng mL^{-1} CEA. All the experiments were performed in 5 mM $K_3[Fe(CN)_6]/K_4[Fe(CN)_6]$–PBS (pH 5.29) at 50 mV s^{-1} scan rate.

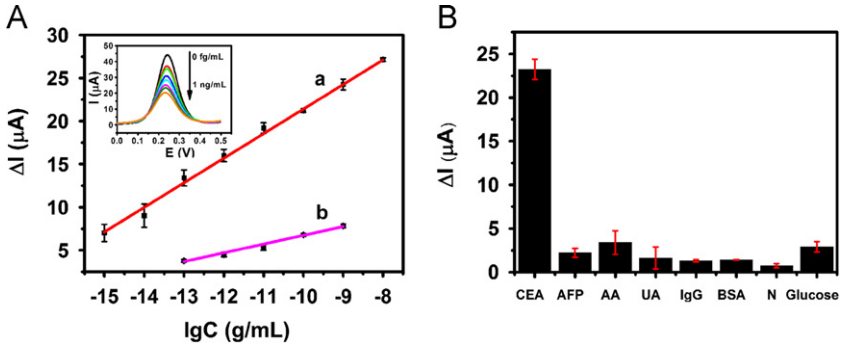

Fig. 4. (A) Calibration plots of (a) GE–PATP–AuNPs–anti-CEA and (b) GE–ATP–AuNPs–anti-CEA. Inset: DPV plots of the immunosensor using PATP–AuNPs–anti-CEA modified GE upon the immersion into varying concentrations of CEA. (B) The interfering effects of other samples on the currents of the immunosensors. Histogram of *N* represents the influence of nonspecific adsorption of CEA when the electrode modified without anti-CEA. The concentration of all the samples was 1 ng mL^{-1}.

3.5.4. *Effect of temperature on the immunoreactions*

As well known, incubation temperature is an important factor for the reaction between antigen and antibody. Fig. 3C shows the effect of temperature on the performance of the immunoassays from 15 to 45 °C. The current responses showed a rapidly decrease to 37 °C and after that it increased with the temperature over 37 °C. That means it would take 37 °C to form the maximum amount of immunocomplexes between the antigens in the incubating solution and antibodies on the electrode surface. Therefore, incubation temperature of 37 °C was adopted as the optimum immunoreaction temperature.

3.5.5. *Effect of incubation time on the immunoreactions*

The effect of the immunochemical incubation time on response signals was also studied. Fig. 3D reveals the influence of incubation time of the immunoassay. The modified electrode was immersed in 1 ng mL^{-1} CEA for 5, 10, 15, 20, 25, 30, 35, 40 and 45 min. The current responses decreased with the incubation time reduced to 35 min and then tended to level off. That means the interaction between antigens and antibodies was not completely until the incubation time up to 35 min. Thus, 35 min was adopted as the optimal incubation time for subsequent study.

3.6. *Analytical performance of the electrochemical immunoassays*

3.6.1. *DPV response and calibration curve*

Under optimal conditions, the sensitivity and dynamic range of the immunoassay were evaluated toward CEA standards. As shown in Fig. 4A (a), the response signal exhibited a wide linear dynamic range from 1 fg mL^{-1} to 10 ng mL^{-1}, with a low detection limit of 0.015 fg mL^{-1}CEA at a signal-to-noise ratio of 3. The linear regression equation is $\Delta I = 49.95 + 2.854\ \lg C$ (g mL^{-1}, $R = 0.9984$). Comparative study was carried out using immunosensor with ATP–AuNPs–anti-CEA modified GE electrode (Fig. 4A (b)). The linear range was 100 fg mL^{-1}–1 ng mL^{-1} and the linear regression equation is $\Delta I = 16.89 + 1.015\ \lg C$ (g mL^{-1}, $R = 0.9940$) with a detection limit of 1.36 fg mL^{-1} ($S/N = 3$). The proposed

immunosensor exhibited higher sensitivity, wider linear range and a lower detection limit. The reason might be that the conducting long-chain polythiols adopted the standing up configuration to provide more sites to immobilize AuNPs accompanied by more anti-CEA and faster electron transfer rate which resulted in the enhanced sensitivity (Jensen et al., 2009).

3.6.2. Repeatability and selectivity of the immunoassay

The repeatability of the immunosensors was examined by analysis of the same concentration of CEA (1 ng mL^{-1}) using five equally prepared electrodes. The five immunosensors, made independently, showed the changes in current responses (ΔI) of 24.26, 23.24, 24.45, 24.97, and 23.82 μA. It was observed that the immunosensor had good repeatability with a relative standard deviation of 2.7% (less than 5.0%).

In order to evaluate selectivity of the developed immunosensor for CEA, the changes in the current responses (ΔI) induced by some possible interferences, such as UA, IgG, glucose, AFP, BSA, and AA were measured. Significantly, the current response for target CEA was much higher than those of others (Fig. 4B), showing that there was a good selectivity of the immunosensor. To address the nonspecific adsorption of antigen, the following control experiment was performed. The GEs, which were modified with PATP–AuNPs and blocked with 1% BSA, were directly used to detect 1 ng mL^{-1} CEA. The changes of the current responses (ΔI) induced by nonspecific adsorbed CEA was only about 0.7 μA, which was much smaller than that (about 23 μA) for the detection of the same concentration of CEA using the electrode modified with anti-CEA, showing that the amount of nonspecific adsorption of CEA was negligible as shown in histogram of *N* in Fig. 4B.

3.6.3. Analysis of real samples

In order to evaluate the effect of the present method to detect real samples, the CEA concentrations in clinical serum samples were measured using the present biosensor and compared with the reference values obtained from MPEI by Automatic Analyzer of Abbott Laboratories in Beijing Deyi Diagnostics (Table 1). The results obtained by present biosensor are well consistent with the data determined by MPEI, showing that the biosensor can be practically applied in clinical analysis to detect the concentration of CEA.

4. Conclusions

In this study, a multifunctional conducting polymer, PATP, was synthesized by the chemical polymerization process and combined with AuNPs to fabricate a novel, sensitive, and label-free amperometric immunosensor for detection of CEA by successfully immobilization of anti-CEA on the GE–PATP–AuNPs electrode. The PATP not only acted as an amplifier to provide signal amplification in the recognition process through the conducting long-chain thiols but also provided tenacious attachment to the electrode due to the multiple thiols groups. The immunosensors exhibited wide linear range (1 fg mL^{-1}–10 ng mL^{-1}) and low detection limit (0.015 fg mL^{-1}). Meanwhile, the electrochemical immunosensor was applied for the determination of clinical serum specimens, and the results were in accordance with those of the commercially available MPEI. The present method could be of significance to be widely applied to other clinical research of important biological molecules.

Table 1
Comparison of clinical serum CEA levels determined using two methods.

Serum samples	1	2	3
Present immunosensor (ng mL^{-1})	5.15	5.00	3.50
MPEI (ng mL^{-1})	5.48	5.25	3.46
Relative deviation (%)	−6.0	−4.8	1.2

Acknowledgment

This research was financed by Grants from the National Natural Science Foundation of China (21273153) and National Natural Science Foundation of Beijing Municipality (2132008).

Appendix A. Supporting information

Supplementary information associated with this article can be found in the online version at http://dx.doi.org/10.1016/j.bios.2013.02.016.

References

Addato, M.A.F., Rubert, A.A., Benítez, G.A., Fonticelli, M.H., Carrasco, J., Carro, P., Salvarezza, R.C., 2011. Journal of Physical Chemistry C 115, 17788–17798.
Bain, C.D., Troughton, E.B., Tao, Y.T., Evall, J., Whitesides, G.M., Nuzzo, R.G., 1989. Journal of the American Chemical Society 111, 321–335.
Crooks, R.M., Ricco, A.J., 1998. Accounts of Chemical Research 31, 219–227.
Cai, X.J., Baldelli, S., 2011. Journal of Physical Chemistry C 115, 19178–19189.
de Boer, B., Meng, H., Perepichka, D.F., Zheng, J., Frank, M.F., Chabal, Y.J., Bao, Z., 2003. Langmuir 19, 4272–4284.
Frens, G., 1973. Nature Physical Science 241, 20–22.
Giberson, R.T., Demaree, R.S., 1994. Microscopy Research and Technique 27, 355–357.
Han, J., Dai, J., Li, L.Y., Fang, P., Guo, R., 2011. Langmuir 27, 2181–2187.
Hartlen, K.D., Ismaili, H., Zhu, J., Workentin, M.S., 2012. Langmuir 28, 864–871.
Henglein, A., Mulvaney, P., Linnert, T., 1991. Faraday Discussions 92, 31–44.
Jensen, G.C., Yu, X., Gong, J.D., Munge, B., Bhirde, A., Kim, S.N., 2009. Journal of Nanoscience and Nanotechnology 9, 249–255.
Johnson, P.A., Levicky, R., 2003. Langmuir 19, 10288–10294.
Kyprianou, D., Guerreiro, A.R., Nirschl, M., Chianella, I., Subrahmanyam, S., Turner, A.P.F., Piletsky, S., 2010. Biosensors and Bioelectronics 25, 1049–1055.
Larson-Smith, K., Pozzo, D.C., 2012. Langmuir 28, 13157–13165.
Lawson, L., Huser, T., 2012. Analytical Chemistry 84, 3574–3580.
Luo, Y.C., Do, J.S., 2004. Biosensors and Bioelectronics 20, 15–23.
Masson, J.F., Battaglia, M., Davidson, J., Kim, Y., Prakash, A.M.C., Beaudoin, S., Booksh, K.S., 2005. Talanta 67, 918–925.
Mustafa, G., Hussain, M., Iqbal, N., Dickert, F.L., Lieberzeit, P.A., 2012. Sensors and Actuators B 162, 63–67.
Noguchi, T., Anzai, J.I., 2006. Langmuir 22, 2870–2875.
Nuzzo, R.G., Fusco, F.A., Allara, D.L., 1987. Journal of the American Chemical Society 109, 2358–2368.
Pchelintsev, N.K., Vakurov, A., Millner, P.A., 2009. Sensors and Actuators B 138, 461–466.
Porter, M.D., Bright, T.B., Allara, D.L., Chidsey, C.E.D., 1987. Journal of the American Chemical Society 109, 3559–3568.
Riepl, M., Mirsky, V.M., Novotny, I., Tvarozek, V., Rehacek, V., Wolfbeis, O.S., 1999. Analytica Chimica Acta 392, 77–84.
Robinson, J.M., Takizawa, T., Vandre, D.D., 2000. Journal of Microscopy 199, 163–179.
Rouhana, L.L., Moussallem, M.D., Schlenoff, J.B., 2011. Journal of the American Chemical Society 133, 16080–16091.
Santos, H.A., Chirea, M., Vladimir, G.M., Sliva, F., Manzanares, J.A., Kontturi, K., 2005. Journal of Physical Chemistry B 109, 20105–20114.
Sergeyeva, T.A., Lavrik, N.V., Piletsky, S.A., 1996. Sensors and Actuators B 343, 283–288.
Shi, W.T., Ma, Z.F., 2010. Biosensors and Bioelectronics 26, 1098–1103.
Sun, F., Grainger, D.W., Castner, D.G., Leach-Scampavia, D.K., 1994. Macromolecules 27, 3053–3062.
Thipmanee, O., Samanman, S., Sankoh, S., Numnuam, A., Limbut, W., Kanatharana, P., Vilaivan, T., Thavarungkul, P., 2012. Biosensors and Bioelectronics 38, 430–435.
Tsai, Y.C., Li, S.C., Chen, J.M., 2005. Langmuir 21, 3653–3658.
Vercelli, B., Zotti, G., Berlin, A., 2007. Chemistry of Materials 19, 443–452.
Vitaliano, R., Fratoddi, I., Venditti, I., Roviello, G., Battocchio, C., Polzonetti, G., Russo, V.M., 2009. Journal of Physical Chemistry A 113, 14730–14740.
Wang, J., 2006. Biosensors and Bioelectronics 21, 1887–1892.
Wang, R.M., Chen, X., Ma, J., Ma, Z.F., 2013. Sensors and Actuators B 176, 1044–1050.
Wang, R.M., Di, J., Ma, J., Ma, Z.F., 2012. Electrochimica Acta 61, 179–184.
Wu, J., Tang, J.H., Da, Z., 2006. Biosensors and Bioelectronics 22, 102–108.

Xiao, N., Yu, C.X., 2010. Analytical Chemistry 82, 3659–3663.
Xiao, X.Y., Pan, S.L., Jang, J.S., Fan, F.R.F., Bard, A.J., 2009. Journal of Physical Chemistry C 113, 14978–14982.
Yang, M., Tsang, E.M.W., Wang, Y.A., 2005. Langmuir 21, 1858–1865.
Yokota, S., 1988. Journal of Histochemistry and Cytochemistry 36, 107–109.
Zengin, H., Zhou, W., Jin, J., Czerw, R., Smith, J.D.W., Echegoyen, L., Carroll, D.L., Foulger, S.H., Ballato, J., 2002. Advanced Materials 14, 1480–1483.